



Data quality control and tools in passive seismic experiments exemplified on Czech broad-band seismic pool MOBNET in the AlpArray collaborative project

Luděk Vecsey¹, Jaroslava Plomerová¹, Petr Jedlička¹, Helena Munzarová¹, Vladislav Babuška¹ and the
5 AlpArray Working Group*

¹Institute of Geophysics of the Czech Academy of Sciences, 14131 Prague, Czech Republic

* www.alparray.ethz.ch

Correspondence to: Luděk Vecsey (vecsey@ig.cas.cz)

Abstract. This paper focuses on major issues related to data reliability and MOBNET network performance in the AlpArray
10 seismic experiments, in which twenty temporary broad-band stations of the Czech MOBNET pool of mobile stations have
been involved. Currently used high-resolution scientific methods require high-quality data recorded for a sufficiently long
time interval at observatories and during full time of operation of temporary stations. In this paper we present both new
hardware and software tools that help to assure the high-quality standard of broad-band seismic data. Special attention is
15 paid to issues like a detection of sensor mis-orientation, timing problems, exchange of record components and/or their
polarity reversal, sensor mass centring, or anomalous channel amplitudes due to, e.g., imperfect gain. Thorough data-quality
control should represent an integral constituent of seismic data recording, pre-processing and archiving, especially for data
from temporary stations in passive seismic experiments. Large international seismic experiments require enormous efforts of
scientists from different countries and institutions to gather hundreds of stations to be deployed in the field during a limited
time period. In this paper, we demonstrate beneficial effects of the procedures we have developed for having a sufficiently
20 large set of high-quality and reliable data from each group participating in field experiments.

1 Introduction

Data from passive seismic experiments of different lateral extent, with densely distributed stations, became crucial source of
information for the modern research of the Earth interior. The USArray (www.usarray.org) or IberArray
(iberarray.ictja.csic.es; Díaz et al., 2010) represent the large-scale temporary networks, whereas, e.g., TRANSALP
25 (Lippitsch et al., 2003) or BOHEMA (Plomerová et al., 2007) belong to small-size passive experiments in central Europe.
Participants of the AlpArray project, the European collaborative geoscience initiative (AlpArray Seismic Network, 2015;
www.alparray.ethz.ch), deployed the largest network of temporary broad-band station ever realized in Europe. The project
focuses on the structure and evolution of the lithosphere-asthenosphere system beneath the greater Alpine area – the Alps
and their forelands. The northern foreland of the Alps is formed by the Bohemian Massif, the easternmost outcrop of the



Variscan belt of the European plate. The project uses seismological as well as associated Earth science data for better understanding the geodynamics of the greater Alpine area and its seismic hazard. The area, studied by generations of geoscientists, comprises the orogenic system, where two large plates (Europe and Africa) have converged and interacted over time with several micro-plates of oceanic and continental provenances (Kissling et al., 2006; Handy et al., 2010 for reviews). Besides the Alpine structure itself, the Alps-Appennines, Alps-Dinarides and Alps-Bohemian Massif contacts in depth are of the particular interest within the AlpArray study. In addition to structural studies related to the orogenic system dominating Europe with the use of associated Earth sciences data (such as gravity, electro-magnetics, geology, etc.), several other topics as seismotectonics and earthquake hazard belong to the core of the project.

To achieve objectives of the project, it is necessary to apply various geological/geophysical imaging methods on data recorded by a homogeneous network of broad-band (BB) seismic stations in the greater Alpine area (Fig. 1). Though the area is in some parts densely covered by permanent seismic observatories, their distribution is far from being homogeneous. Therefore, the distribution of ~360 existing permanent stations have been complemented by ~260 temporary BB stations to create a relatively dense network of unprecedented large scale in Europe, with homogeneous station spacing of about 50 km.

The station spacing and station location is designed in such a way that for any site in the Alpine region there is always a station of the AlpArray Seismic Network (AASN) at a distance up to ~26 km. The temporary seismic network of such large extent requires intensive collaboration between many institutions (currently more than 45 institutions from 17 countries), combination of individual national/institutional seismic pools of temporary stations and coordination of their deployment, keeping the high-level maintenance and experienced handling. Thanks to the large extent of the array and density of the stations, results from seismic tomography and several other techniques applied on data collected during the unique passive experiment will shed light on the detailed 3D architecture of the crust and upper mantle. The project aims at imaging structures and understanding processes from the Earth's surface down to ~600 km in the mantle of this extremely complicated orogenic region.

The AlpArray area, set as a region delimited by a 250 km distance from the 800 m altitude isoline surrounding the Alps, covers a large portion of the Czech (CZ) part of the Bohemian Massif (BM). Ten BB observatories of the Czech Regional Seismological Network (CRSN), one permanent BB station of the West Bohemian Network (WEBNET) along with 20 temporary BB stations of the pool of seismic stations from MOBNET of the Institute of Geophysics, Czech Academy of Sciences (IG CAS), cover the area with the spacing required (Fig. 1). The Czech team of the AASN (coded Z3 in the European Integrated Data Archive (EIDA) system) is responsible for the deployment and maintenance of the MOBNET stations in the Czech part of the AlpArray, as well as for completeness and correctness of recorded seismic data, transferred to the EIDA centres. Data from the Czech temporary stations of the Z3 networks code (www.fdsn.org/networks/detail/Z3_2015/), with the access restricted according to the AlpArray rules, are transferred to



ODC (www.orfeus-eu.org/data/eida/nodes/), while data from the Czech permanent stations with open access continue being stored in the GEOFON (geofon.gfz-potsdam.de).

Main purpose of this paper is to describe technical parameters of the MOBNET stations, to present newly developed control units for setting sensor and data acquisition systems (DAS) and to document significance of careful data-quality control, which could help other groups of the AlpArray project in preparing their seismic data for archiving. Special attention is paid to detection of sensor mis-orientation, timing problems, exchanged of components and/or their polarity reversal, mass centring problems, or anomalous channel amplitudes due to, e.g., an imperfect gain. Elimination of all these concerns is of the extreme importance for keeping the high quality of archived seismological data, which is crucial for success of the AlpArray project, as well as of any passive seismic experiment.

2 Deployment of MOBNET stations within the AlpArray project

Twenty stations of the MOBNET pool have been deployed in the Bohemian Massif (BM) since August 2015, as a part of the AASN (Fig. 2). Before, the stations had been deployed for approximately one-year period during 2014-2015 in the Eastern Alpine Seismic Investigation (EASI) project, the first implemented AlpArray Complementary Experiment (Table 1, see Fig. 1). The EASI transect was composed of 55 broadband seismic stations, configured in a zig-zag pattern on either side of the central longitude line of 13.35° E, with the north-south distance between stations of 10 km. The transect spanned a region of ~540 km long, between the Erzgebirge Mts. at the Czech-German border in the North and the Adriatic Sea, near Trieste in the South. The distance of each station to either side of the central line was ~6 km. We followed the general recommendations of the Technical strategy of the AlpArray (www.alparray.ethz.ch) and kept the stations within 1.5 km of the target location, if topographic, field and infrastructure conditions allowed.

The northernmost stations AAE01-AAE20 (Fig. 2) of the MOBNET pool involved in the AlpArray–EASI were equipped mostly with the STS-2 seismometers, two CMG-3T and three CMG-3ESP seismometers, and the GAIA DAS. The stations were installed preferably in vaults of castles/chateaux, churches, or suitable abandoned buildings. Figure 3 shows an example of a station location, seismometer installation, quality of the site and, noise level, etc. (see also S1-S19, supplements). Keeping notation of Molinari et al. (2016), we can characterize the location as of urban free-field site, only exceptionally as of building site (Table 1). The stations ran at the autonomous regime and reported daily their state-of-health in SMS messages. Altogether, we recorded 280 GB of data stored in mseed which contribute to the AlpArray-EASI studies including tomography, ambient noise analysis and receiver functions, considering anisotropy in all three types of investigations, as well as in shear-wave splitting analyses. The depth range of scientific investigations encompasses the crust and the mantle lithosphere, down to the lithosphere-asthenosphere boundary (LAB).



The EASI field measurement was finished in August 2015 and twenty MOBNET stations were re-installed at new sites, selected according to the AASN geometry (see Fig. 2). With the exception of A090A, all other stations operate offline. Data from the offline stations are recorded on flash cards with capacity exceeding at least 4 times space needed for data sampled at rate of 100 sps and collected in three-month intervals to be checked and supplied to the ODC-EIDA node. Similarly to the
5 EASI transect, most of the AASN-CZ sites are of urban free-field types (Table 1, Fig. 4, S20-S38). Though the region of the BM is densely populated with local industrial and agricultural sources of high-frequency noise, the stations meet requested noise limits (Peterson, 1993) as it is shown for the example in Figure 4 (see also S20-S38). Only at about 30 % of stations, noise exceeds the limit on vertical components at long-period range ($T > 100$ s) (e.g., S33). Some of the stations exhibit distinct seasonal variations of noise level, which results in exceeding the noise limit in the long-period range on horizontal
10 components (Fig. 5), (Wolin et al., 2015).

Figure 6 shows current status of data availability from the MOBNET stations included in the AlpArray passive field experiment. Data recorded by GAIA stations are stored at sampling rate of 100 sps on flash cards with capacity of recordings exceeding 3-4 times the three-month interval of data collection. In case of the AlpArray-EASI complementary project in
15 2014-2015, we retrieved 96 % of the data at each station, on average (Fig. 6a). As concerns the ongoing AlpArray project, the data completeness is 99 % (for period by October 2016) for the MOBNET stations. Several gaps in data were caused by summer thunderstorms that damaged electrical supplies (Fig. 6b). Though almost all our stations operate offline, the data completeness for MOBNET stations in the AASN is similar to that for stations of the Austrian or Swiss parts of the AASN with an online data transmission (Fuchs et al., 2016; Molinari et al., 2016).

20 **3 Seismometer and GAIA control and calibration devices**

Our broad-band temporary stations involved in the AlpArray project are equipped mostly with broad-band seismometers STS-2 and several CMG (Table 1), and with data acquisition systems GAIA developed by the VISTEC company (www.vistec.cz). To assure high-degree reliability of the seismometer-DAS pairs performance, we have developed four special control devices for seismometers of different types and one for the GAIA DAS. In general, these boxes generate
25 pulses into the systems and compare amplitudes of input and output signals. The devices enable to calibrate sensors and data acquisition systems, as well as to check in-situ gain of all individual components and polarity of the recorded signal. The hardware check facilitates identification/verification of any malfunction of the systems and enables their immediate treatment, often directly in the field.

3.1 Guralp host box (CMG-3T and CMG-3ESP(C))

30 Guralp host box (Fig. 7a) becomes an integral constituent of each seismometer CMG-3T and CMG-3ESP(C) and it is an analogy of the hand-held unit of the Guralp company provenience, or the host box of the STS-2 seismometer. Our Guralp



host box is incorporated between the seismometer and the GAIA DAS, and enables fundamental handlings of the seismometer, namely pendulums arrestment (lock/unlock) and their centring. Busy LED light informs about state of the seismometer. The host box is equipped with a connector for the Guralp control and calibration unit (see Sect. 3.2), or for a remote seismometer control (e.g., via GSM).

5 **3.2 Guralp control and calibration unit (CMG-3T and CMG-3ESP(C))**

This device (Fig. 7b) enables to calibrate a seismometer by the unit step signal or Dirac delta pulse. It has also an input for external calibrating signal of an arbitrary shape. Polarity of the calibrating signal can be changed and the signal size can be altered in two levels. There is a switch between the calibration mode and the display mode of pendulum positions of the Z, NS and EW components. A push button centres the pendulums.

10 **3.3 Guralp centring unit (CMG-40T)**

Guralp centring unit (Fig. 7c) was developed for seismometer pendulums without electronic centring, e.g., CMG-40T. For the pendulum position checking, it is necessary to disconnect the seismometer from the DAS and to connect the Guralp centring unit. Deviation of the pendulum from the central position is proportional to the mass position voltage. Pendulum centring requires the mass position voltage close to zero. The unit has a built-in accumulator, which supplies energy to
15 seismometer during the control. In case of insufficient accumulator capacity, the accumulator can be plug-in via an external charger. The Guralp centring unit, developed for seismometers with only manual pendulum centring, can be used also for pendulum position check of seismometers with electronic control, but then the centring unit does not enable pendulum centring.

3.4 STS-2 control and calibration unit

20 STS-2 control and calibration unit (Fig. 7d) has been developed for centring pendulums and for seismometer calibration. The device is being connected to the “Monitor” connector of the host box provided by the seismometer producer. The host box forms the integral part of the system, through which the STS-2 seismometers is supplied with electric energy. The STS-2 control and calibration unit displays positions of the pendulums for the U, V and W components, or offsets of the standard Z, NS, EW components of the output signal. The unit is equipped with a button of automatic centring of pendulum position
25 (auto-zero push button), connected in parallel to similar button of the host box. The 120 s / 1 s switch of the control and calibration unit changes modes between the broad-band and short-period regime.

Each of the U, V and W components can be calibrated separately with the unit step signal or the Dirac delta pulse. There is also a switch for an external calibrating signal of an arbitrary shape, e.g., of a sinusoidal signal. If the components are calibrated together, calibration currents and their polarities are chosen so that the output signals (components Z, NS, EW)
30 have the same amplitudes and polarities. This procedure guarantees correct functioning of the seismometer.



3.5 GAIA gain and calibration unit

GAIA gain and calibration unit (Fig. 7e) checks and calibrates inputs into the GAIA DAS, but it can be used for calibration of any type of digitizers as well (Kinematics, Nanometrics, Reftek, Guralp etc.), after being equipped with corresponding connector reductions. The unit enables to calibrate analogue inputs, to set order of channels, to evaluate cross-talks between the channels, to measure channel amplification and sensitivity (the gain, i.e., the counts to voltage conversion). Number of channels undergoing calibration and channel polarity can be changed. Differential mode and the plus or minus single-ended regimes can be switched over. The calibration is done by voltage jump of a known size. Built-in generator of saw-shape calibrating voltage serves for a judgement of linearity of the input signal.

4 Data quality control and assurance

10 Currently used high-resolution seismological methods require high-quality data inputs. The high level of data quality has to be stable during a long-time interval for seismological observatories and for a full time of operation of temporary stations within passive experiments. Data quality control represents the necessary step for achievement of the high-quality seismic data. We differentiate (1) in-situ controls with technical equipment, applied during installation of stations and their servicing, and (2) ex-post software controls, applied on downloaded data.

15 4.1 Seismic noise

Identification of ambient noise conditions is nowadays a standard procedure when searching sites suitable for station installation. However, the level of ambient noise has to be watched continuously, to monitor potential changes in conditions of recordings, or to detect technical problems of a station. According to the AlpArray working group requirements average noise level should be 20 dB lower than the New High Noise Model (NHNM; Peterson, 1993) on all components within the 20 1-10 Hz frequency range. The same noise level is requested only for the vertical component in the long-period range (30-200 s). Because ambient noise is usually higher on horizontal components, an average noise level is recommended to be only 10 dB less than the NHNM. To follow the ambient noise level, we use the seismic probabilistic power spectral density (PPSD) procedure by McNamara and Buland (2004) and Custodio et al. (2014) which is a part of ObsPy module (Krischer et al., 2015).

25 Figure 8 shows the PPSD medians for all MOBNET stations included in both configurations within the AlpArray project. While the level of noise for periods below 10 s fulfils the noise requirements, noise on horizontal components for periods higher than 10 s is often larger, especially in winter time, but still acceptable for temporary deployments. One has to bear in mind that a compromise between optimal site conditions and the required station spacing has to be accomplished. An 30 enhanced thermal insulation of seismometers might decrease the ambient noise level at longer periods. On the other hand,



the difference between the noise levels on horizontal and vertical components can be exploited as one of tools to decipher potential exchange of components, as we describe below.

4.2 Sensor orientation

Exact orientation of seismometers in the geographic co-ordinate system is one of the most important tasks during station
5 installations. Mis-oriented sensors affect results of procedures based on modern three component seismological observations
and can lead to false interpretations (Ekström and Busby, 2008; Vecsey et al., 2014; Wang et al., 2016). Determination of the
northward direction has been routinely done for years with the use of standard compass, with the best accuracy of $\pm 5^\circ$ in case
of no magnetic disturbances in nearby surroundings. However, such accuracy is no more sufficient. The top-level current
practice is to orient seismometers with the use of the high-precision gyrocompass measurement during a station installation
10 and to repeat the measurements during station services. Repeated measurements are desirable to avoid any seismometer mis-
orientation resulting from, e.g., an accidental shift of sensors by a person or an animal, as well as due to a nearby strong
lightning, which all we have experienced. To determine correct sensor orientations, one can use Rayleigh-wave polarization-
angle method (e.g. Stachnik et al., 2012), in which differences between the Rayleigh-wave polarizations and their theoretical
back-azimuths are plotted in dependence on origin times of seismic events. For determining an exact moment of the change
15 of sensor orientation, the Rayleigh-wave polarization-angle method can be combined with daily amplitude-mean plots. After
determining a day, when the sensor happens to be mis-oriented, one has to search changes in the data signal.

When installing our stations for the AlpArray-EASI transect, we oriented the seismometers carefully, but only according to a
standard compass. Later we checked the orientation of all sensors with a fiberoptic gyrocompass. We have found deviations
20 larger than 5° from the true North at 9 of 20 stations (Table 2) and extremely large deviations in orientation at two of them
(AAE13 $N=282^\circ$ and AAE04 $N=341^\circ$). Two other stations (AAE13 and AAE18) changed significantly their orientation
during the experiment: by 8° and 7° , respectively. We have used the polarization-angle method for a rough estimate of a
moment, when orientation of the sensors has been changed, and daily means and signal plots for setting exact time of the
sensor re-orientations.

25 Sensors of all our stations involved in the currently running AASN (A071-A090) have been installed with the use of our
gyrocompass and their orientation is regularly checked. During about a one-year period of the array operation, we have
already recorded three unwanted changes of sensor orientation due to a human intervention. Besides the necessary sensor re-
orientation on spot, previous inaccuracies in sensor orientations have been corrected in the metadata.

30 4.3 Timing issues

Correct timing is crucial for kinematic studies based on exact arrival times of seismic waves. Incorrect time decreases
accuracy of picking individual phases, causes false phase identification or a loss of data at all. Timing errors of 1 s or smaller



are not clearly evident during routine seismological analyses, but can be revealed from station “log” files, if provided by the registration system, from carefully kept service sheets, or from headers of mseed data. Existing time gaps and overlaps can be calculated from the time of the first sample, number of samples and sampling rate in each mseed block.

- 5 Here we address three important timing problems: (1) the leap second recorded with a delay, (2) switch between the UTC and GPS times and (3) malfunction of an oscillator tuning the station time. The leap second is introduced into the Coordinated Universal Time (UTC) usually once or twice per year in order to keep the UTC day time close to the mean solar time. The leap second is usually applied at midnight, while clocks in data acquisition systems are being synchronized later, e.g., with a 30-90 minute delay. Moreover, the leap-second correction is applied at individual stations differently, because
- 10 times of their synchronizations differ. It is thus necessary to shift the leap second right to the midnight for all temporary stations before data archiving.

Sometimes, a problem can arise due to a wrong synchronization of the inner time (UTC) of a station and the GPS time. This can happen when the coordinated universal time in the “almanac” transmitted by satellites disappears from the memory of a

15 station for some reasons (e.g., low voltage of inner battery, incorrect satellite signal recorded, etc.). Currently, the UTC and GPS times differ by 18 seconds. Thus the UTC/GPS time switch results in the 18 s shift of the time in recorded data. Such time shift can last for several hours or a full day and requires to be corrected as well.

Failure of an oscillator tuning the station time could cause a jump or a linear increase of timing error in data. However, such

20 difficulties should occur exceptionally. If it happens and we are able to identify such a problem and reconstruct a real timing, it is necessary to correct times directly in the mseed data, which is more difficult than applying corrections in the metadata. When checking our data, we have found an oscillator failure at station A087A, which resulted in a final time error of 0.18 s during 8 days in October 2015.

4.4 Interchange of components and polarity reversal

- 25 Results from different studies dealing with waveforms, i.e., with amplitudes of seismic waves, sometimes raise a suspicion that the three components of seismograms need not be correctly labelled, i.e., the components could be interchanged. The simplest way to verify the correct indication of the three components is a comparison of waveforms for a selected strong teleseismic event recorded on several nearby stations, which we call the waveform similarity method (Fig. 9a). Several other methods can be used as well, e.g., a visualization of daily means of signal amplitudes, sometimes called offsets (Fig. 9b), or
- 30 a comparison of noise levels on the vertical and horizontal components in PPSD. In case of correct component identification, the noise level on the vertical component should be lower than that on the horizontal components. Correction of exchanged components can be done either in the metadata, or preferably directly in the mseed data.



Reversed polarity of components, arising from different technical reasons, is not as rare as one would expect. Polarity reversal can be easily identified by the waveform similarity method for nearby stations. We can also use a single-station method that is based on a search of Rayleigh wave polarization (the polarization-angle method). Then the differences between the Rayleigh wave polarization and the theoretical back-azimuth are plotted in dependence on theoretical back-azimuths. If only one horizontal component is reversed, the differences change linearly between -180° and $+180^\circ$. The zero difference reflects the fact that the reversed component does not play any role in the component summation and identifies the components with the correct polarity (see Fig. 10a; the EW component is the correct one). In case of the reversed polarity on the Z component, or if both horizontal components are reversed, the differences between the Rayleigh-wave polarizations and the theoretical back-azimuths attain values around 180° for all back-azimuths (Fig. 10b). Moreover, we have identified also an interchange of both horizontal components in combination with their polarity reversals. This complicated case can be solved by combination of the methods mentioned above and by a careful analysis of the results. Similarly to the component interchange, the component reversal can be corrected either in the metadata, or preferably in the mseed data.

4.5 Gain imperfection

Anomalous signal amplitudes due to imperfectly set gains on one or more components are not very frequent in comparison with the sensor mis-orientations, but their danger for data analysis procedures is similarly large. We can recognize anomalously large or low recorded amplitudes in two ways: first, by means of technical devices, such as control and calibration units (see Sect. 3), and second, by means of software methods applied on recorded seismic signals.

The software inspection of the amplitude size is based on evaluation of noise, which is the only continuous signal in seismic data. We have implemented a new method which compares ratios of normalized power spectra between the three components in a range of 4-8 seconds. In this range, the secondary microseisms are substantially larger than noise from local sources. Directionality of the microseisms due to different sources is eliminated by normalizing the spectrum of each trace via an average spectrum calculated over the traces of surrounding stations. The spectra are calculated within certain time intervals, e.g., weeks, months, or a whole time range. Resulting ratios of the spectra provide a running record of individual channel sensitivity and allow us to follow potential changes of the amplitudes in a course of time. In combination with sporadic in-situ gain controls by the Gain and calibration box (Sect. 3.5), we have reliable control of potential anomalous size of recorded amplitudes and thus we can determine when a detected change in the gain occurred.

We document a successful use of the hardware and software methods on data from the two seismic experiments. During the data processing, we have found that the power spectra of the EW components at stations AAE14 (EASI) and A087A (AASN) are lower by approximately 11 dB (Fig. 11a). The NS/Z component ratio is close to zero, while ratios EW/Z and EW/NS, where the EW component is involved, are 10 dB lower. Station documentations identified that stations AAE14 and A087A were equipped with identical sensor and data acquisition system. Therefore, afterwards we tested the gain of each



component of the sensor-DAS pair with the calibration boxes as described in Sect. 3. The test confirmed the amplitudes recorded on the EW component were 3.6 times smaller ($20 \cdot \log 3.6 = 11$ dB) than it should be. The error in the acquisition system was identified and repaired. If such error is identified by an in-situ measurement, then it can be immediately eliminated (DAS can be repaired or changed, as it was possible in case of running station A087A). Metadata of A087A for a previous period, as well as the metadata of the AAE14 station active in the finished EASI measurements were corrected subsequently. In another case we have found that either the amplitudes on EW components are about two-times larger, or the gains of the NS and Z components are lower by ~ 6 dB at stations AAE15 (EASI) and A088A (AlpArray) (Fig. 11b). Results of the normalized PPSD ratios are only relative ones. The absolute value - the half-size gain compared with the declared one, was identified by an in-situ measurement with the use of the STS-2 control and calibration unit (see Sect. 3.4). Source of the low gain was localized in a defect cable of the seismometer. The double-checked gain levels of each component (by the hardware unit and by the software calculating the normalized PPSD ratios) enabled us to correct reliably the gains in the station metadata files and thus to correct anomalous amplitudes.

4.6 Drift of sensor mass position

One of artefacts seen in the PPSD reflects a failure of the automatic mass re-centring of the sensor (McNamara and Buland, 2004). If a seismometer is not able to correct a drift of the mass position itself, amplitudes of seismic signals become saturated. Signal corresponding to such a time period has a characteristic “flat” spectrum shape (Fig. 12a). The flat course in an interval of ~ 0.3 -50 s differs clearly from the shape of the noise distribution modulated by secondary microseisms. The large undesirable drift of the mass position from its central position limits the dynamic range of the sensor and therefore, it needs to be identified as soon as possible. Running information about a sensor mass “drift” comes from the size of a sum of counts in one-hour interval on each component provided by GAIA DAS in daily SMS reports. Besides this hardware checks, daily means of recorded amplitudes (Fig. 12b) serve as an independent fast and easy tool for ex-post identification of the mass centring problem. Moreover, complementing the daily amplitude means by their standard deviations and absolute values of daily amplitude extremes (maxima or minima) we can better assess the state of health of each station (Fig. 12c).

5 Conclusions

We have developed both the hardware and software tools to contribute with reliable high-quality waveform data to passive seismic experiments. At present, twenty broad-band stations of the Czech MOBNET pool of temporary stations are incorporated in the AlpArray Seismic Network. The stations were also deployed in the preceding AlpArray EASI complementary experiment. To assure high-degree reliability of the STS-2/CMG seismometer-DAS pairs performance, we have developed four special control devices for seismometers of different types and one for the GAIA DAS. The devices calibrate both the sensors and data acquisition systems in-situ and check gain and polarity of all components. We emphasise the importance of precise sensor orientation by a gyrocompass both during station installations and of its regular checks



during the field measurements. Information extracted from power spectra density, spectra ratios, daily amplitude means and other parameters, followed by the designed procedures in routine data processing, allow us to identify several problems, e.g., imperfectly set gains, interchange of components and polarity reversals, insufficient sensor mass centring and last, but not the least, time issues. The hardware control in-situ and the ex-post software data checking represent the double check of data quality. The former removes problems immediately in the field, the latter allows restoring data back in time, until the moment when a problem occurred. We believe that the newly developed control and calibration units for setting sensor-DAS systems and the documentation of the significance of careful data-quality control, could be helpful for other groups participating in collaborative passive seismic experiments.

Data availability

10 Data from the MOBNET pool as a part of the AlpArray project is stored in EIDA (www.orefus-eu.org/eida/), currently with restricted access (<http://www.alparray.ethz.ch/research/complementary-experiments/easi/data-access-citation/> and http://www.alparray.ethz.ch/seismic_network/backbone/data-access/).

Team list

The complete member list of the AlpArray Working Group can be found at <http://www.alparray.ethz.ch>.

15 Acknowledgements

Cooperation with participants of the AlpArray projects is greatly appreciated. The research of the Czech team was supported by grants No. M100121201 of the Czech Academy of Sciences and partly by No. P210-12-2381 of the Grant Agency of the Czech Republic. Data acquisition from permanent observatories was supported by the project of Large research infrastructure CzechGeo/EPOS, grants Nos. LM2010008 and LM2015079. Several figures and calculations have been prepared with the use of the Generic Mapping Tools (Wessel and Smith, 1998) and ObsPy (Krischer et al., 2015).

References

AlpArray Seismic Network: Eastern Alpine Seismic Investigation (EASI) - AlpArray Complementary Experiment, AlpArray Working Group, Other/Seismic Network, doi:10.12686/alparray/xt_2014, 2014.
AlpArray Seismic Network: AlpArray Seismic Network (AASN) temporary component, AlpArray Working Group, Other/Seismic Network, doi:10.12686/alparray/z3_2015, 2015.



- Custódio, S., Dias, N. A., Caldeira, B., Carrilho, F., Carvalho, S., Corela, C., Díaz, J., Narciso, J., Madureira, G., Matias, L., Haberland, Ch., and WILAS Team: Ambient noise recorded by a dense broadband seismic deployment in Western Iberia, *B. Seismol. Soc. Am.*, 104, 2985–3007, doi:10.1785/0120140079, 2014.
- Díaz, J., Villaseñor, A., Morales, J., Pazos, A., Cordoba, D., Pulgar, J., García-Lobón, J. L., Harnafí, M., Carbonell, R., Gallart, J., and TopoIberia Seismic Working Group: Background noise characteristics at the IberArray broadband seismic network, *B. Seismol. Soc. Am.*, 12, 618–628, doi:10.1785/0120090085, 2010.
- Ekström, G., and Busby, R. W.: Measurements of seismometer orientation at USArray transportable array and backbone stations, *Seismol. Res. Letters*, 79, 555–561, doi:10.1785/gssrl.79.4.554, 2008.
- Fuchs, F., Kolínský, P., Gröschl, G., Bokelmann, G., and the AlpArray Working Group: AlpArray in Austria and Slovakia: technical realization, site description and noise characterization, *Adv. Geosci.*, 43, 1–13, doi:10.5194/adgeo-43-1-2016, 2016.
- Handy, M. R., Schmid, S. M., Bousquet, R., Kissling, E., and Bernoulli, D.: Reconciling plate-tectonic reconstructions of Alpine Tethys with the geological–geophysical record of spreading and subduction in the Alps, *Earth-Science Reviews*, 102, 121–158, doi: 10.1016/j.earscirev.2010.06.002, 2010.
- Kissling, E., Schmid, S. M., Lippitsch, R., Ansorge, J., and Fügenschuh, B.: Lithosphere structure and tectonic evolution of the Alpine arc: new evidence from high-resolution teleseismic tomography, in: D. Gee, R.A. Stephenson (Eds.), *European Lithosphere Dynamics*, Geological Society London, Memoirs 32, 129–145, 2006.
- Krischer, L., Megies, T., Barsch, R., Beyreuther, M., Lecocq, T., Caudron, C., and Wassermann, J.: ObsPy: a bridge for seismology into the scientific Python ecosystem, *Computational Science & Discovery*, 8, 014003, doi:10.1088/1749-4699/8/1/014003, 2015.
- Lippitsch, R., Kissling, E., and Ansorge, J.: Upper mantle structure beneath the Alpine orogen from high-resolution teleseismic tomography, *J. Geophys. Res.*, 108 (B8), 2376, doi:10.1029/2002JB002016, 2003.
- Molinari, I., Clinton, J., Kissling, E., Hetényi, G., Giardini, D., Stipčević, J., Dasović, I., Herak, M., Šipka, V., Wéber, Z., Gráczér, Z., Solarino, S., the Swiss-AlpArray Field Team, and the AlpArray Working Group: Swiss-AlpArray temporary broadband seismic stations deployment and noise characterization, *Adv. Geosci.*, 43, 15–29, doi:10.5194/adgeo-43-15-2016, 2016.
- McNamara, D. E., and Buland, R. P.: Ambient noise levels in the continental United States, *B. Seismol. Soc. Am.*, 94, 1517–1527, doi:10.1785/012003001, 2004.
- Peterson, J.: Observations and modeling of seismic background noise, USGS Open-File report, 93–322, 1993.
- Plomerová, J., Achauer, U., Babuška, V., Vecsey, L., and BOHEMA working group: Upper mantle beneath the Eger Rift (Central Europe): plume or asthenosphere upwelling?, *Geophys. J. Int.*, 169, 675–682; doi:10.1111/j.1365-246X.2007.03361.x, 2007.



- Stachnik, J.C., Sheehan, A. F., Zietlow, D. W., Yang, Z., Collins, J., and Ferris, A.: Determination of New Zealand Ocean Bottom Seismometer Orientation via Rayleigh-Wave Polarization, *Seismol. Res. Letters*, 83 (4), 704–713, doi:10.1785/0220110128, 2012.
- Vecsey, L., Plomerová, J., Babuška, V., and PASSEQ Working Group: Mantle lithosphere transition from the East European Craton to the Variscan Bohemian Massif imaged by shear-wave splitting, *Solid Earth*, 5, 779–792, doi:10.5194/se-5-779-2014, 2014.
- 5 Wang, X., Chen, Q. F., Li, J., and Wei, S. J.: Seismic Sensor Misorientation Measurement Using P-Wave Particle Motion: An Application to the NECsaids Array, *Seismol. Res. Letters*, 87 (4), 901–911, doi:10.1785/0220160005, 2016.
- Wessel, P., and Smith, W. H. F.: New, improved version of the Generic Mapping Tools released, *Eos T. AGU*, Volume 79, 10 579, 1998.
- Wolin, E., van der Lee, S., Bollmann, T. A., Wiens, D. A., Revenaugh, J., Darbyshire, F. A., Frederiksen, A. W., Stein, S., and Wyssession, M. E.: Seasonal and diurnal variations in long-period noise at SPREE stations: the Influence of soil characteristics on shallow stations performance, *B. Seismol. Soc. Am.*, 105, 2433–2452, doi:10.1785/0120150046, 2015.

15



Net work	Station	Latitude	Longitude	Elevation (m)	Site name	Housing type	Sensor ground	Sensor	Datalogger	Start time
XT	AAE01	50.6075	13.4320	590	Hora Sv. Kateriny	adit	concrete on bedrock	STS-2 120s	GAIA-2T	2014-07-23
.	STS-2 120s	Quan330S	2014-11-21
XT	AAE02	50.5107	13.2526	843	Hora Sv. Sebastiana	building/cellar	concrete	STS-2 120s	GAIA-1	2014-06-24
XT	AAE03	50.4306	13.4300	305	Drouzkovice	building	concrete	CMG-40T 30s	GAIA-1	2014-06-24
XT	AAE04	50.3545	13.2588	388	Uhostany	church	stone floor	STS-2 120s	GAIA-3	2014-07-26
XT	AAE05	50.2522	13.3696	301	Krasny Dvur	castle	stone floor	STS-2 120s	GAIA-1,2T	2014-07-01
XT	AAE06	50.1747	13.2520	545	Valec	castle/cellar	stones in cement	CMG-3T 120s	GAIA-1,2T	2014-07-01
XT	AAE07	50.0733	13.4219	455	Ostrovec	church	stone floor	STS-2 120s	GAIA-1	2014-07-01
XT	AAE08	49.9910	13.2322	409	Manetin	castle	concrete	STS-2 120s	GAIA-1	2014-07-17
XT	AAE09	49.8890	13.4135	493	Obora	church	tiles on concrete	STS-2 120s	GAIA-1	2014-07-04
XT	AAE10	49.7998	13.2509	353	Ceminy	castle	concrete	STS-2 120s	GAIA-1,2	2014-07-04
XT	AAE11	49.7030	13.4692	345	Stary Plzenec	church	stone floor	STS-2 120s	GAIA-1	2014-06-20
XT	AAE12	49.6045	13.2629	360	Dnesice	building/cellar	concrete	STS-2 120s	GAIA-1	2014-07-10
XT	AAE13	49.5289	13.4547	480	Lazne Letiny	building	tiles on concrete	STS-2 120s	GAIA-1	2014-06-20
XT	AAE14	49.4427	13.2495	386	Dolany	church	tiles on concrete	STS-2 120s	GAIA-2	2014-07-04
XT	AAE15	49.3648	13.4141	680	Zdeborice	church	stone floor	STS-2 120s	GAIA-1	2014-07-17
XT	AAE16	49.2642	13.2193	643	Depoltice	church	tiles on concrete	STS-2 120s	GAIA-1	2014-07-10
XT	AAE17	49.1554	13.4379	890	Dobra Voda	church	brick floor	CMG-3ESP 30s	GAIA-1	2014-06-17
XT	AAE18	49.0982	13.2165	685	Schwellhausl	cellar	concrete	STS-2 120s	GAIA-1	2014-08-28
XT	AAE19	48.9712	13.4825	1175	Breznik	building	tiles	CMG-3ESP 30s	GAIA-1	2014-06-16
XT	AAE20	48.8896	13.2981	615	Eppenschlag	building	concrete	STS-2 120s	GAIA-1	2014-08-21
Z3	A071A	49.7419	12.6911	502	Stare Sedliste	church	stone floor	CMG-3T 120s	GAIA-1	2015-10-27
Z3	A072A	49.4683	13.1735	495	Chudenice	castle/cellar	stones in cement	STS-2 120s	GAIA-2T,1	2015-08-27
Z3	A073A	49.9916	13.2331	407	Manetin	castle/cellar	stones in cement	STS-2 120s	GAIA-1	2015-09-23
Z3	A074A	49.6715	13.5309	385	Kozel	building	tiles on concrete	STS-2 120s	GAIA-1	2015-10-02
Z3	A075A	50.0377	13.8737	285	Krivoklat	building	concrete	STS-2 120s	GAIA-1	2015-10-06
Z3	A076A	49.6168	14.1494	532	Makova Hora	church	concrete on bedrock	CMG-3T 120s	GAIA-1	2015-09-08
Z3	A077A	49.2705	14.0739	370	Kestrany	castle/cellar	protrusion wall	CMG-3ESP 30s	GAIA-1	2015-11-03
Z3	A078A	48.8640	14.2845	1060	Klet	urban free field	concrete	CMG-3ESP 30s	GAIA-1	2015-10-20
Z3	A079A	49.2288	14.7074	438	Drachov	church	stone floor	STS-2 120s	GAIA-1	2015-10-15
Z3	A080A	49.6840	14.9288	502	Loreta	building	concrete	STS-2 120s	GAIA-1	2015-10-12
Z3	A081A	50.0752	15.0341	228	Dobrichov	building	stones in cement	STS-2 120s	GAIA-1	2015-09-25
Z3	A082A	50.0610	15.6502	220	Zivanice	church	concrete	STS-2 120s	GAIA-1	2015-10-08
Z3	A083A	49.6959	15.6077	573	Cachotin	church	tiles on concrete	STS-2 120s	GAIA-1	2015-10-16
Z3	A084A	48.9434	15.7007	403	Bitov	castle	tiles on concrete	STS-2 120s	GAIA-1	2015-09-22
Z3	A085A	49.4392	16.1962	458	Strazek	church	tiles on concrete	STS-2 120s	GAIA-1	2015-10-07
Z3	A086A	49.8528	16.1457	391	Nove Hradky	castle/cellar	stone on bricks	STS-2 120s	GAIA-1	2015-09-19
Z3	A087A	49.7049	16.8893	430	Bouzov	castle	tiles on concrete	STS-2 120s	GAIA-3	2015-09-19
Z3	A088A	49.4303	17.2911	211	Tovacov	castle	concrete	STS-2 120s	GAIA-1	2015-09-24
Z3	A089A	49.1521	17.0920	263	Nesovice	castle/cellar	concrete	STS-2 120s	GAIA-1	2015-11-08
Z3	A090A	49.3655	17.8278	659	Maruska	underground shelter	concrete in soil	CMG-3ESP 30s	GAIA-1	2015-09-24
.	CMG-40T 30s	GAIA-1	2015-12-02
.	CMG-3ESP 30s	GAIA-1	2016-04-06

Table 1: List of Czech temporary stations involved in the AlpArray-EASI complementary experiment (network code XT) and the AlpArray Seismic Network (AASN) (code Z3).



EASI stations (CZ)	Re-measured -	Sensor re-	Re-measured -	Difference [deg]
	original installation with compass [deg]	orientation to N acc. to gyrocompass [deg]	end of registration [deg]	
AAE01	359.9	359.9	x	x
AAE02	7.4	0.4	0.4	0
AAE03	4.0	359.8	0.7	0.9
AAE04	x	x	340.8	x
AAE05	357.1	359.3	0.6	1.3
AAE06	3.2	0.9	0.9	0
AAE07	355.6	0.4	2.6	2.2
AAE08	358.0	0.6	0.8	0.2
AAE09	2.1	0.3	359.6	-0.7
AAE10	8.7	0.4	3.1	2.7
AAE11	5.2	0.7	359.5	-1.2
AAE12	2.9	0.7	359.5	-1.2
AAE13	282.0	0.7	352.3	-8.4
AAE14	2.3	359.5	357.2	-2.3
AAE15	3.2	359.9	359.4	-0.5
AAE16	2.2	359.4	0.5	1.1
AAE17	6.2	0.2	0.8	0.6
AAE18	7.2	0.4	6.9	6.5
AAE19	6.0	359.8	359.6	-0.2
AAE20	3.5	0.2	0.4	0.2

Table 2: Gyrocompass measurements of sensor orientations during the AlpArray-EASI complementary experiment. The largest errors are highlighted.

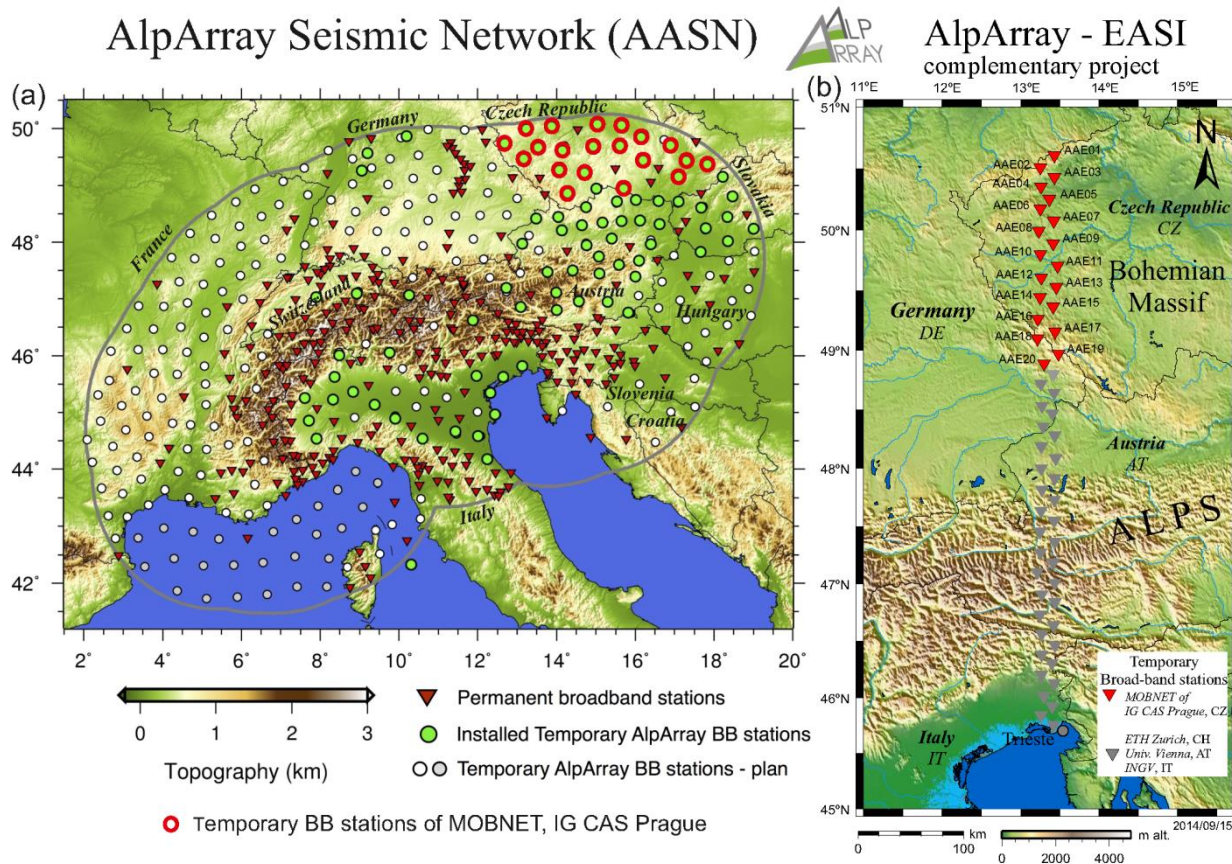


Figure 1: Broad-band stations of the Czech MOBNET pool in the AlpArray collaborative project – (a) within the AlpArray Seismic Network and (b) within the AlpArray-EASI complementary project.

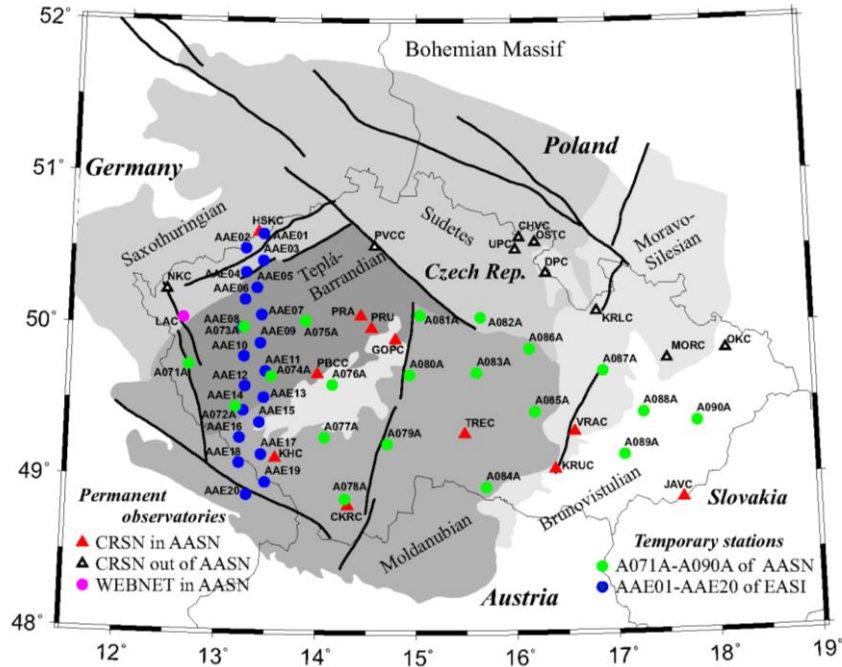


Figure 2: Schematic map of major tectonic units of the Bohemian Massif and seismic stations involved in the AlpArray project.

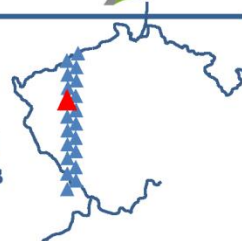


AAE08
Manětín

INSTALLATION

EQUIPMENT

Start : 17.7.2014 Sensor : STS 2 120 s
 Stop : 23.9.2015 Depth : 0m
 Lat : 49.9910 Recorder : Gaia 1
 Lon : 13.2322 Power : electricity grid
 Alt : 409 m Data : miniSeed, 6 GB



The station is located in the former stables of Manětín chateau.
 Seismometer is built on a concrete floor.
 The GPS antenna is brought out through the window, length - 5 m, direction - S, view partially obscured.
 Geomorphology: Rakovník Uplands.
 Subsoil: phyllite.

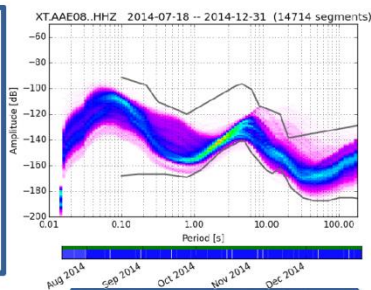


Figure 3: Example of installation of one of the broad-band MOBNET stations in the AlpArray-EASI experiment - AAE08 Manětín.



A076A
Maková Hora

INSTALLATION

EQUIPMENT

Start : 8.9.2015
 Lat : 49.6168
 Lon : 14.1494
 Alt : 532 m

Sensor : CMG-3T 120 s
 Depth : 3 m
 Recorder : Gaia 1
 Power : electricity grid



The station is located on the lower ground floor of the former rectory pilgrimage church at Maková Hora (Poppy Mountain). Upper ground floor is occasionally used for recreational purposes. Seismometer is installed in the shaft on concrete pillars built on bedrock. The GPS antenna is brought out through the window, length - 5 m, direction - S, view open. Geomorphology: Benešov Uplands. Subsoil: orthogneiss.

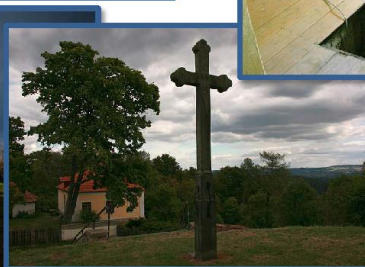
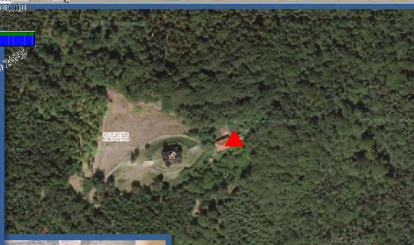
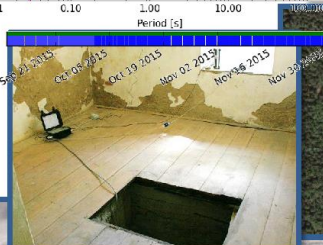
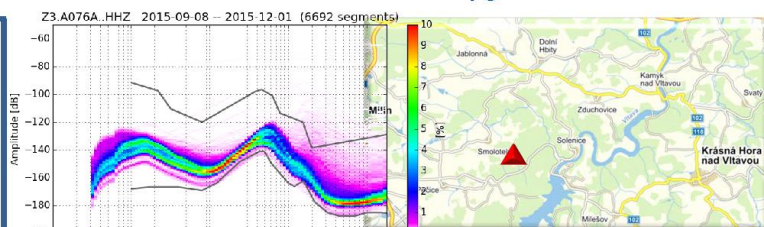


Figure 4: Example of installation of one of the broad-band MOBNET stations in the AlpArray Seismic Network (AASN) - A076A Maková Hora.

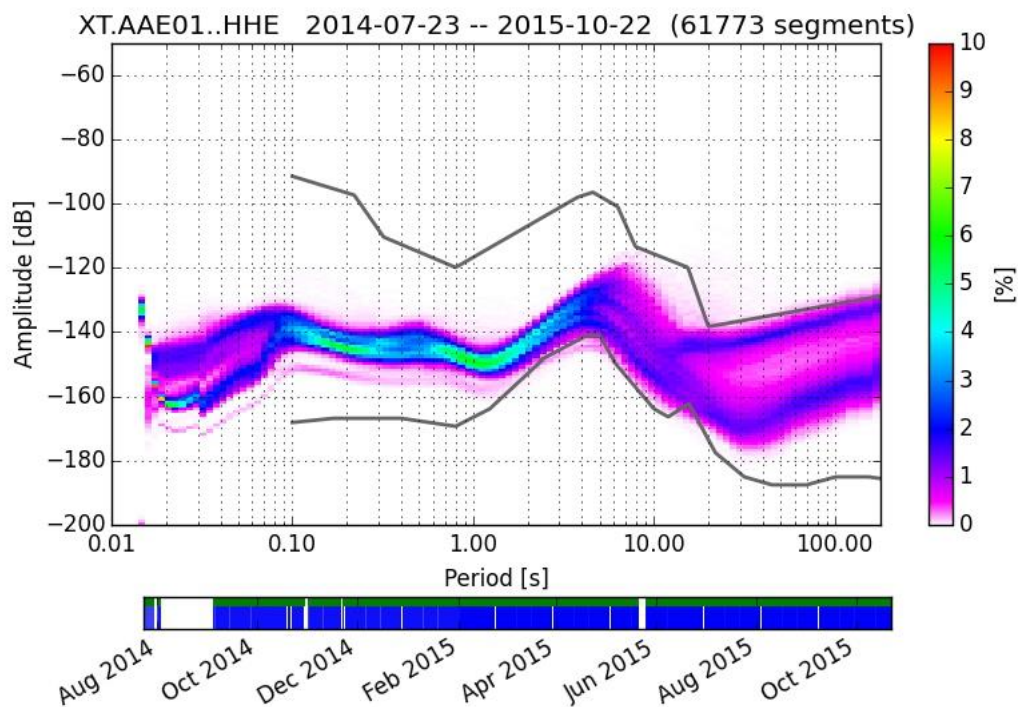


Figure 5: Probabilistic power spectra density on the horizontal component of the AAE01 station of the AlpArray-EASI experiment. The example shows a noise level during the winter time relative to low-noise level during the summer period, in which the noise is far below the limit of the noise model (grey curves; Peterson, 1993).

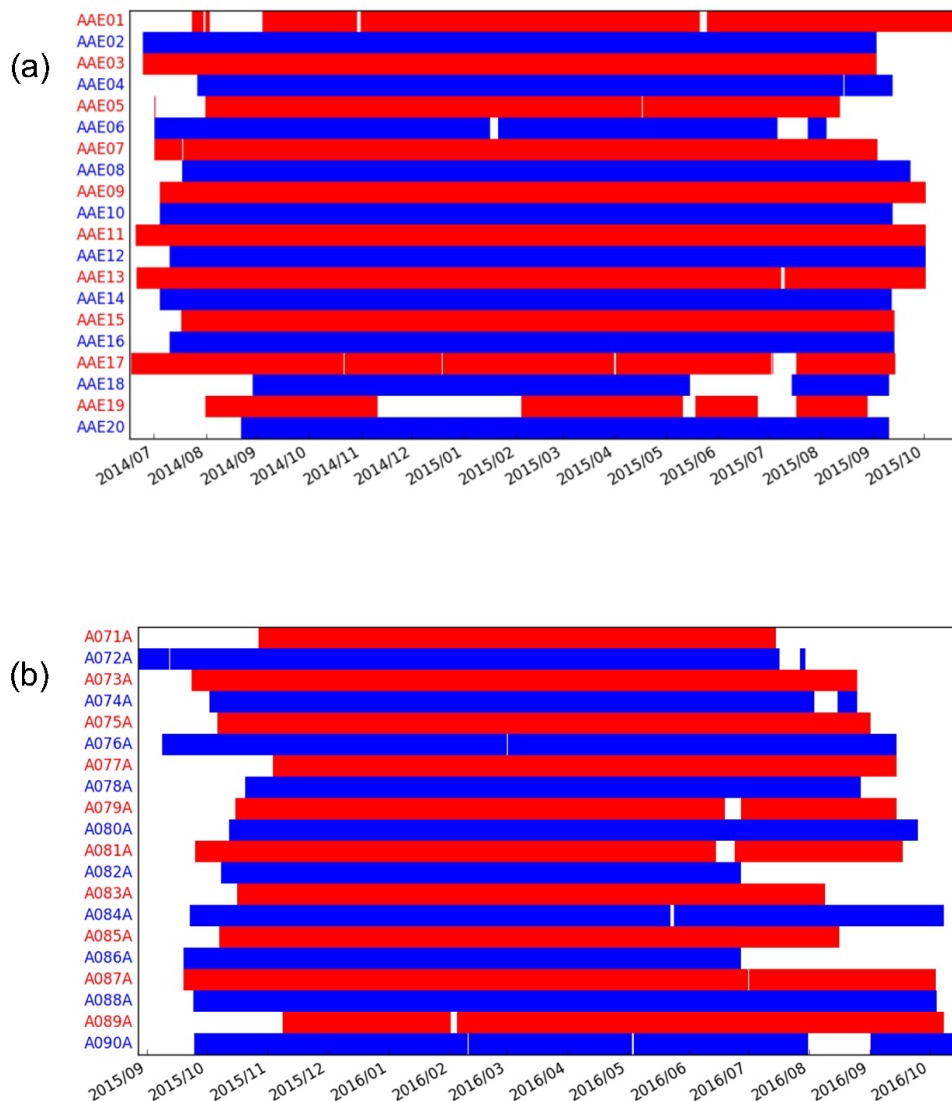


Figure 6: Data completeness of MOBNET stations in the AlpArray projects: (a) in the EASI complementary field measurements and (b) in the ongoing AlpArray experiment.

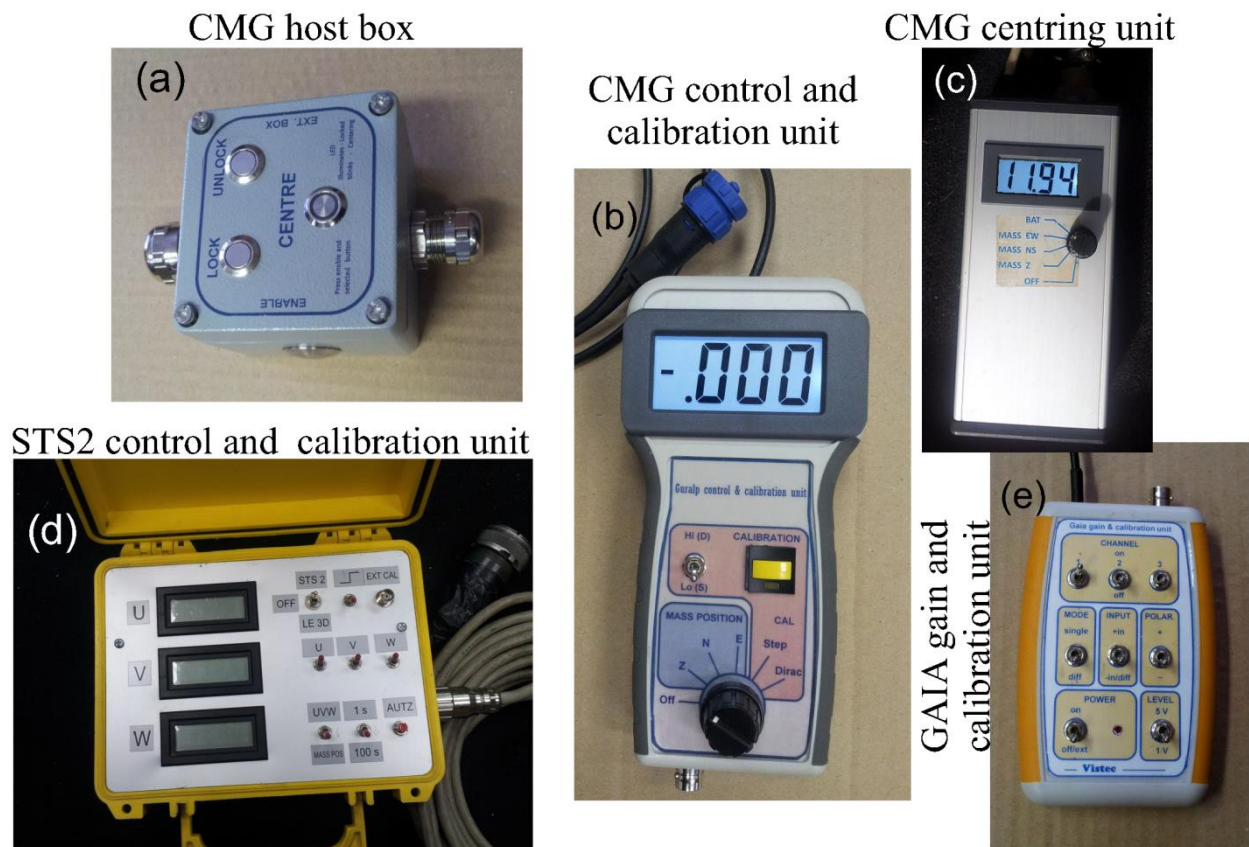


Figure 7: Control and calibration units developed for the broad-band seismometers and GAIA DAS to guarantee the high-quality of recorded data.

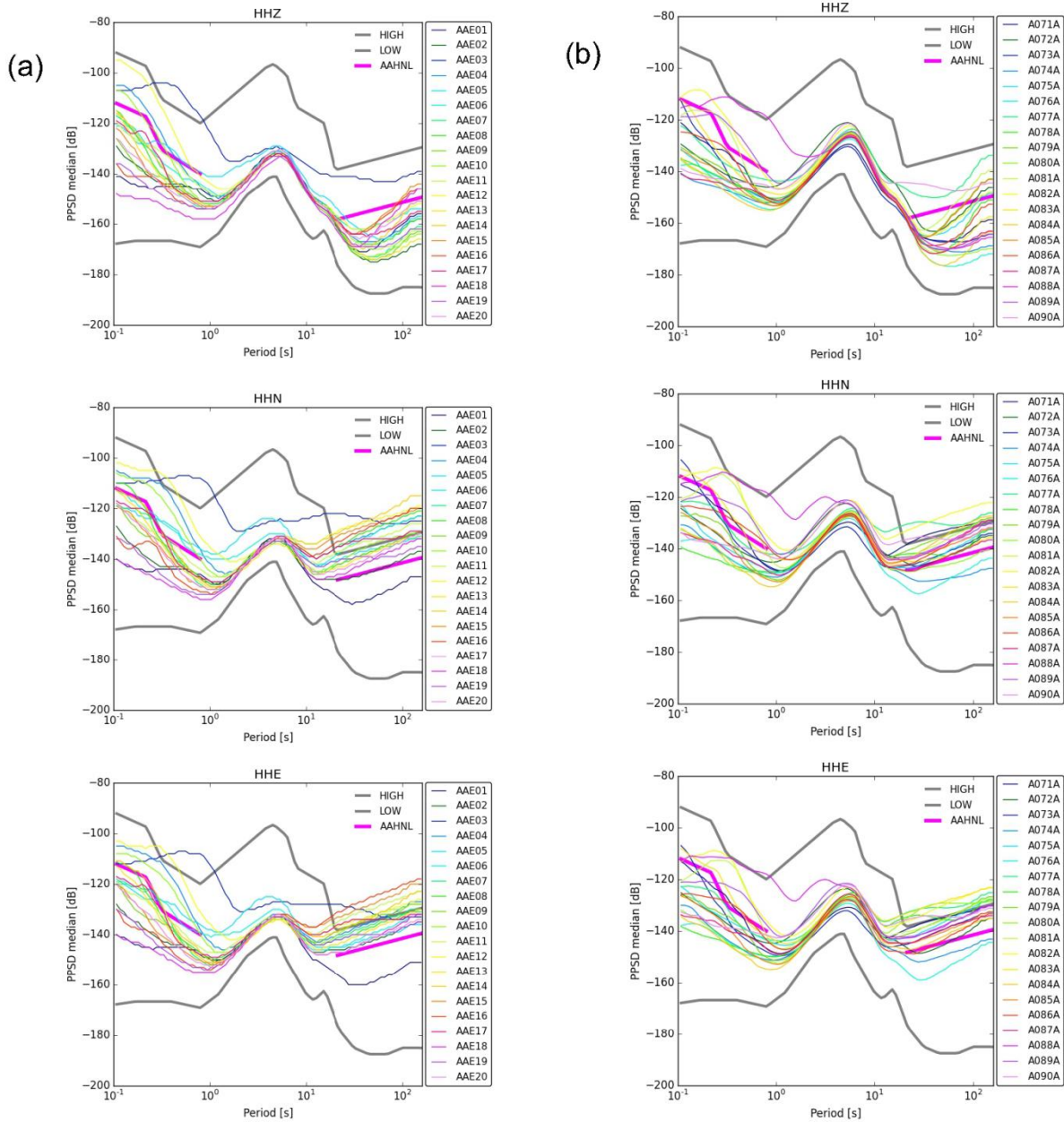


Figure 8: Medians of probabilistic power spectral density (PPSD) of seismic noise at the MOBNET stations involved (a) in the AlpArray-EASI complementary experiment and (b) in the AlpArray Seismic Network (AASN). The thick red line marks the upper limit of recommended noise level between the low- and high-noise level models (Peterson, 1993).

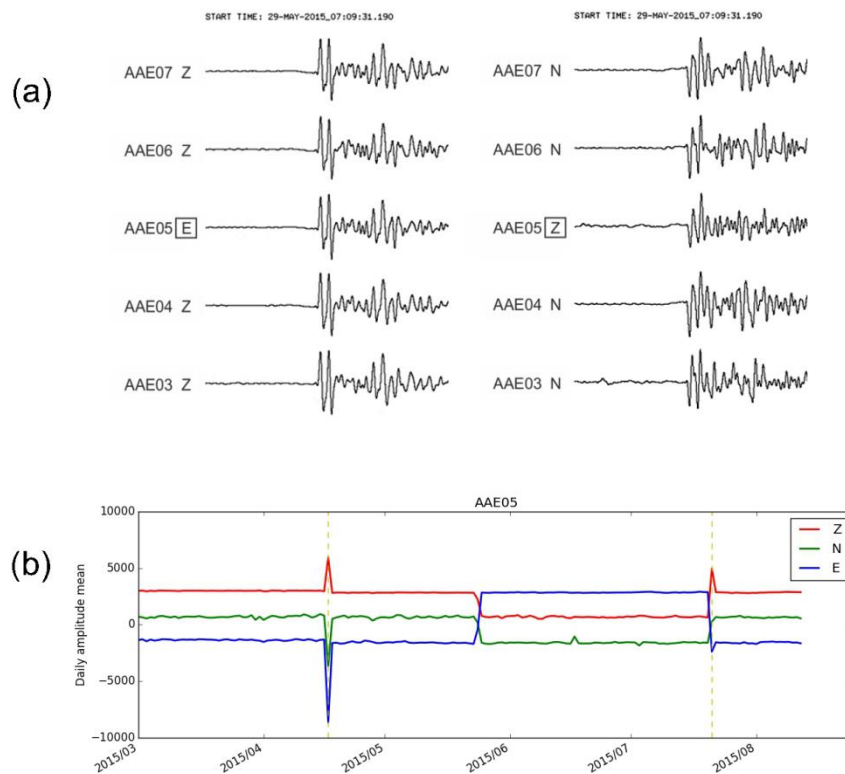
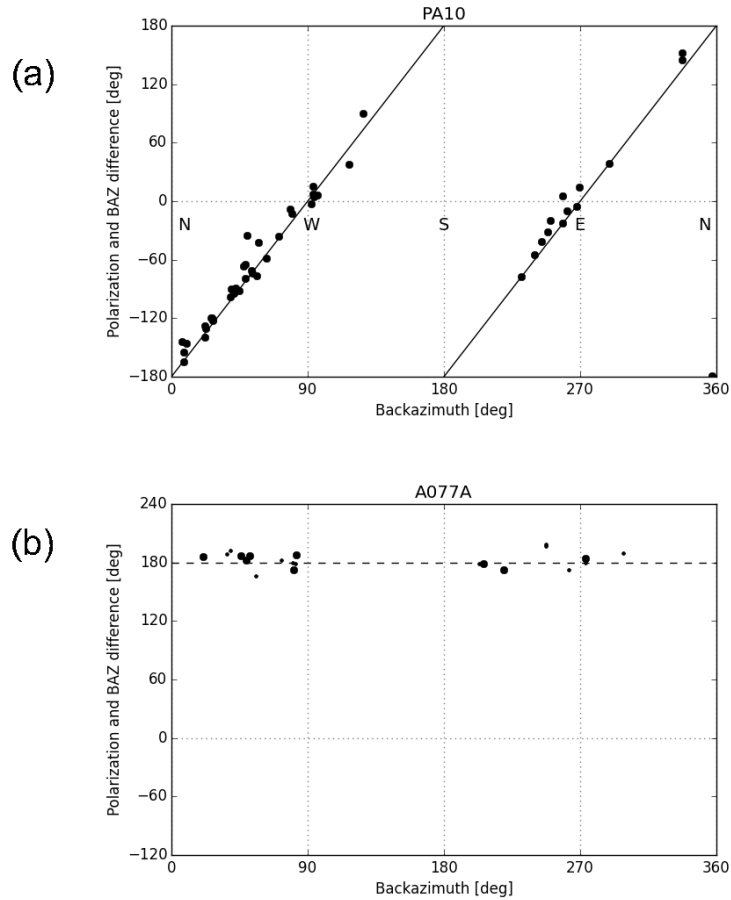


Figure 9: The waveform similarity method showing the interchange of the EW and Z components (a) at the AAE05 station. Daily amplitude means (b) of all three components at the AAE05 station during June – July, 2015 indicated the interchange of all three components. Vertical dashed lines show dates of station servicing.



5 **Figure 10: Differences between the Rayleigh wave polarizations and event theoretical back-azimuths (BAZ) in dependence on the theoretical back-azimuth. Linear dependence of the difference (a) identifies the polarity reversal of the NS component. Polarization of waves arriving from the East or West is not affected by the reversed NS component. Station PA10 of the PASSEQ experiment 2006-2008 (Vecsey et al., 2014) is used as an example. (b) Constant difference of $\sim 180^\circ$ corresponds to the polarity reversal of both horizontal components at the A077A station of AASN.**

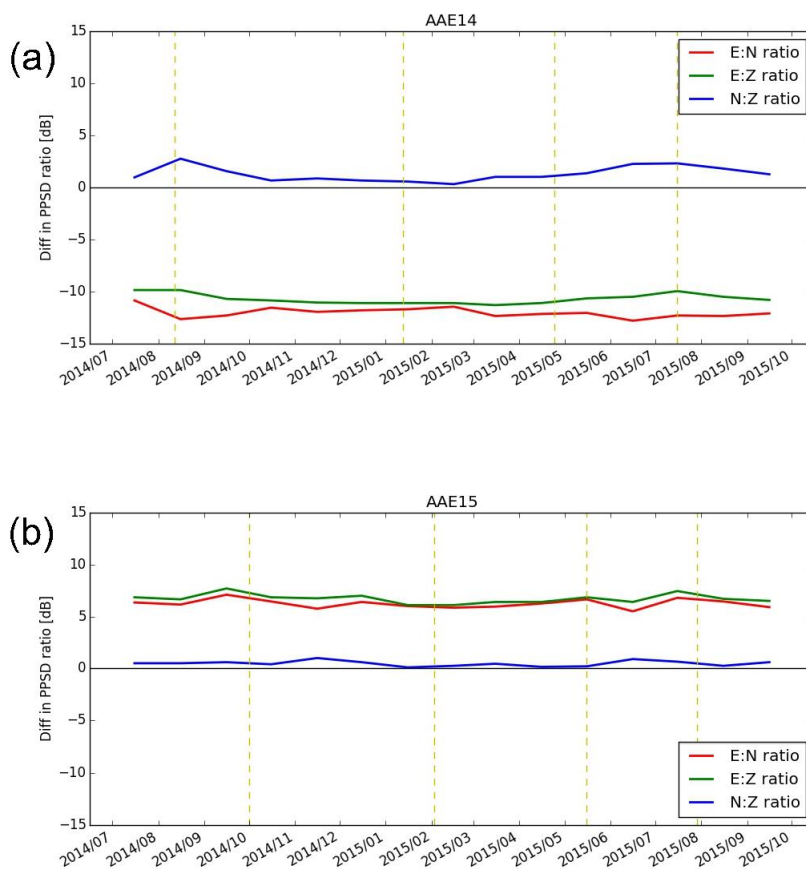


Figure 11: Seismometer gain check. Monthly averages of normalized power spectra ratios identify imperfect gains of the EW component (a) and of both the NS and EW components (b).

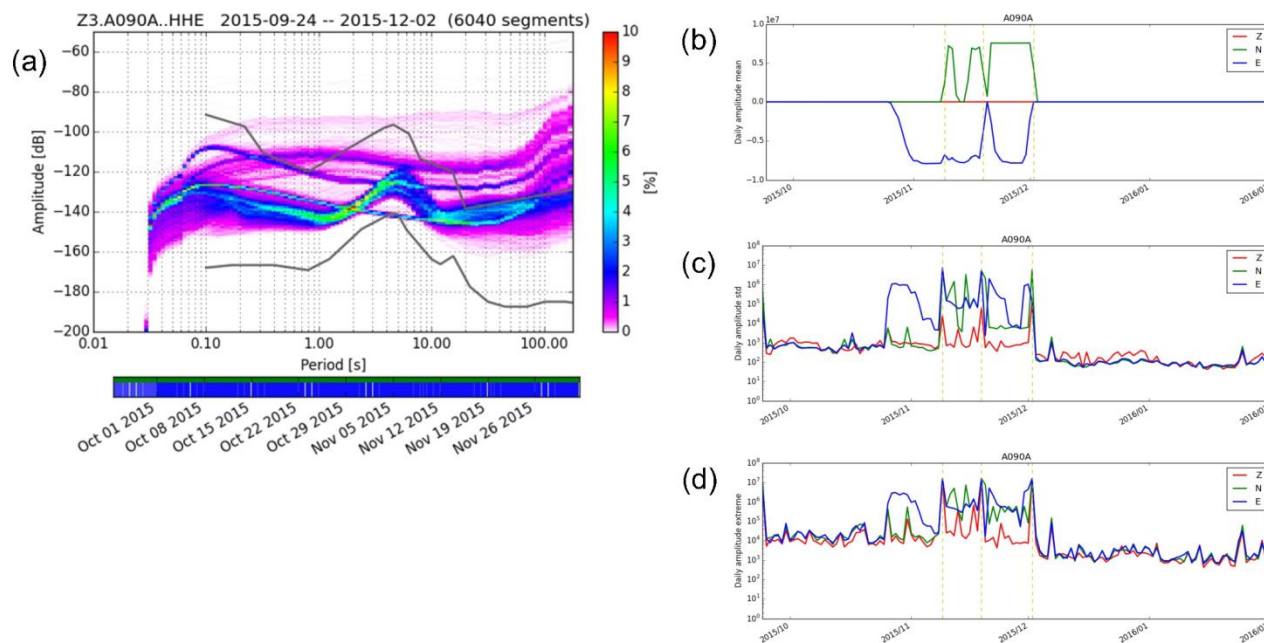


Figure 12: Sensor mass centring. Flat curves in PPSD (a), daily means of amplitudes (b), their standard deviations (c) and absolute values of daily amplitude extreme (d) identify the failure of the automatic mass re-centring.